Title	Effects of absorption and inhibition during grating formation in photopolymer materials
Authors(s)	Gleeson, M. R.; Kelly, John V.; Close, Ciara E.; O'Neill, Feidhlim T.; Sheridan, John T.
Publication date	2006-10-01
Publication information	Journal of the Optical Society of America B, 23 (10): 2079-2088
Publisher	Optical Society of America
Link to online version	http://dx.doi.org/10.1364/JOSAB.23.002079
Item record/more information	http://hdl.handle.net/10197/3382
Publisher's statement	This paper was published in Journal of the Optical Society of America B and is made available as an electronic reprint with the permission of OSA. The paper can be found at the following URL on the OSA website: http://www.opticsinfobase.org/abstract.cfm?URI=josab-23-10-2079. Systematic or multiple reproduction or distribution to multiple locations via electronic or other means is prohibited and is subject to penalties under law.
Publisher's version (DOI)	10.1364/JOSAB.23.002079

Effects of absorption and inhibition during grating formation in photopolymer materials

Michael R. Gleeson, John V. Kelly, Ciara E. Close, Feidhlim T. O'Neill, and John T. Sheridan

School of Electrical, Electronic and Mechanical Engineering, College of Engineering, Mathematical and Physical Sciences, University College Dublin, Belfield, Dublin 4, Ireland

Received February 28, 2006; revised June 28, 2006; accepted June 29, 2006; posted July 6, 2006 (Doc. ID 68367)

Photopolymer materials are practical materials for use as holographic recording media, as they are inexpensive and self-processing (dry processed). Understanding the photochemical mechanisms present during recording in these materials is crucial to enable further development. One such mechanism is the existence of an inhibition period at the start of grating growth during which the formation of polymer chains is suppressed. Some previous studies have indicated possible explanations for this effect and approximate models have been proposed to explain the observed behavior. We examine in detail the kinetic behavior involved within the photopolymer material during recording to obtain a clearer picture of the photochemical processes present. Experiments are reported and carried out with the specific aim of understanding these processes. The results support our description of the inhibition process in an acrylamide-based photopolymer and can be used to predict behavior under certain conditions.

OCIS codes: 090.0090, 090.2900, 090.2890, 160.5470.

1. INTRODUCTION

Photopolymer materials have the ability to optically record high-diffraction-efficiency, low-loss, volume holographic gratings in self-processing materials and are of ever-increasing commercial importance. Improving their characteristics, to attain the full potential of these materials, requires the development of accurate models, validated using reproducible experimental data sets, which can ultimately provide clear insight into the photochemical processes involved during recording. Exploration of the kinetics involved in the recording of holographic gratings is an integral part of this work. In this paper the photochemical kinetics involved during recording in our acrylamide-based photopolymer[1] material is examined. Specifically we aim to better understand what takes place inside the material during exposure, i.e., to explain the effects of the variation of the absorbance of the photosensitive dye with time and the suppression of radical production due to the presence of inhibitors. By improving the physical accuracy of our model, and understanding the relationship between the rate of polymerization and the concentrations of monomer, polymer, dye, initiator, and inhibitor, we aim in this paper to improve the validity of the one-dimensional polymerization-driven diffusion (PPD) model.[2] Development of this model will facilitate the eventual full nonlocal polymerization-driven diffusion (NPDD) modeling of such materials.[3–6]

We proceed as follows. First we examine the photochemical processes involved during grating formation and incorporate the suppression of radical production into the rate equations, which form the basis of our models. We then incorporate the effects of changes in the absorbance of the photosensitive dye during exposure. Having developed appropriate rate equations, we derive and solve the resulting coupled equations numerically.[3–6] A set of experiments is carried out that, following comparison with the model, support the assumptions made in deriving our equations and illustrate the effects associated with the inhibition and bleaching processes.

2. PHOTOCHEMICAL PROCESSES

Assuming bimolecular termination,[5] we begin by discussing radical chain polymerization. In particular we examine polymerization due to photoinitiation and examine the effect on excited dye molecules due to the presence of inhibitors such as oxygen. Furthermore we include the effect of a time-dependent transmittance,[7–9] which describes the change in the material absorption during grating growth.

Free radical polymerization is a chain reaction involving three steps: initiation, propagation, and termination. Initiation involves the production of free radicals,

$$I \xrightarrow{k_d} R^{\bullet}, \tag{1}$$

where k_d is the radical generation rate constant. The rate of this reaction is given by

$$R_d = d[R^{\bullet}]/\mathrm{d}t = k_d[I], \tag{2}$$

where $[R^{\bullet}]$ is the free radical concentration and $[I]$ is the initiator concentration. The free radicals then bind to a monomer M to form the chain initiation species $M_1^{\bullet}$,

$$R^{\bullet} + M \xrightarrow{k_i} M_1^{\bullet}, \tag{3}$$

where k_i is the initiation rate constant. The radical $M_1^{\bullet}$ then propagates by bonding with monomer molecules to form long polymer chains with an active tip known as a macroradical.

$$M_n^{\bullet} + M \xrightarrow{k_p} M_{n+1}^{\bullet}, \tag{4}$$

where k_p is the propagation rate constant and $M_n^{\bullet}$ is a macroradical of n monomeric units where a monomeric unit is the largest constitutional unit contributed by a single monomer molecule.[10] The initiator consists of a photosensitive dye and a reducing agent. The dye can become excited in the presence of a photon and when excited can accept an electron from the reducing agent, i.e., a tertiary amine (triethanolamine),[11] and can then produce a free radical $R^{\bullet}$:

$$\text{dye} + h\nu \rightarrow \text{dye}^{*},$$

$$\text{dye}^{*} + M \rightarrow R^{\bullet}. \tag{5}$$

As the radicals are produced, some of the dye molecules, which are excited, return to their ground state or move to a triplet state:[12]

$$\text{dye}^{*} \xrightarrow{k_f} \text{dye} + h\nu,$$

$$\text{dye}^{*} \xrightarrow{k_{isc}} \text{dye}^{T},$$

$$\text{dye}^{T} + C_I \xrightarrow{k_R} \text{dye}^{\bullet -} + C_I^{\bullet} + H^{+}. \tag{6}$$

An excited dye molecule, which has been promoted to that state due to a photon interaction, can either decay by fluorescence[13] at a rate of k_f back to its ground state or can be excited to a triplet state dye^T by intersystem crossing at a rate of k_{isc}. The excited triplet state can then undergo an electron transfer reaction (rate constant k_R) with the coinitiator C_I, which creates the primary radical $C_I^{\bullet}$, a dye radical $\text{dye}^{\bullet -}$, and a free proton H^{+}.[1,12] The dye radical eventually reacts with other constituents and forms a bleached state.[12] This process results in dye molecules being consumed and can lead to cessation of polymerization if the dye is consumed too quickly.

All of these effects tend to suppress the creation of radicals and therefore slow the rate of polymerization (of monomer). Other contributors to this radical suppression are inhibitors, which are present within the chemicals in our material, and the presence of oxygen, which also acts as an inhibitor.[14–18] We assume that the effect of inhibition during the fabrication process is primarily due to the oxygen present in our material. Therefore we suggest that the oxygen reacts with the excited dye and deactivates it into a passive state;

$$\text{dye}^{*} + \rho \xrightarrow{k_\rho} Y + \rho^{\bullet}, \tag{7}$$

where Y is the photoreduction product and is assumed to only participate once (i.e., its relaxation time is long compared with the exposure time), ρ is the oxygen, and k_ρ is the deexcitation rate of the dye.[14] This effect is present throughout exposure but is most noticeable at the start. The equation governing the removal of excited dye is

$$R_\rho = \frac{\mathrm{d}[Y]}{\mathrm{d}t} = k_\rho[\text{dye}^{*}][\rho], \tag{8}$$

where R_ρ is the rate of removal of free radicals due to the removal of excited dye molecules by oxygen. This process reduces the concentration of excited dye molecules available for creating free radicals. Thus it ultimately reduces the monomer polymerization rate.

The frequency of encounters between the free radicals is another factor determining the rate of polymerization. It can be accounted for using the cage effect.[19] It is assumed that only some fraction f of the free radicals produced will react with the monomer (in the starting reaction).

From Eqs. (2) and (8) we see that the rate of production of free radicals R_r that are responsible for the production of monomer radicals, with the inclusion of the presence of oxygen, can then be given by

$$R_r = fk_d[I] - R_\rho, \tag{9}$$

with the initiator concentration $[I]$. From relation (3) the rate of production of monomer radicals R_i can be written as

$$R_i = \mathrm{d}[M_1^{\bullet}]/\mathrm{d}t = k_i[R^{\bullet}][M], \tag{10}$$

where $[M]$ is the monomer concentration and $[R^{\bullet}]$ is the primary radical concentration. In general the rate of production of monomer radicals R_i is much greater than the rate of production of free radicals R_r; therefore initiator radicals are consumed as fast as they are generated.[6] The rate-determining step is thus the decomposition of the initiator. Initiator radicals are consequently formed with a rate

$$\mathrm{d}[R^{\bullet}]/\mathrm{d}t = R_r - R_i = (fk_d[I] - R_\rho) - k_i[R^{\bullet}][M] = 0. \tag{11}$$

Thus the rate of monomer radical generation R_i is equal to the chain initiation rate and

$$R_i = k_i[R^{\bullet}][M] = fk_d[I] - R_\rho. \tag{12}$$

Chain growth would continue in this way until the supply of monomer is exhausted were it not for the strong tendency of radicals to react in pairs to form paired-electron covalent bonds with the loss of radical activity. At sufficiently low initiator concentrations, chain termination will occur mainly by combination,[6,19]

$$M_n^{\bullet} + M_m^{\bullet} \xrightarrow{k_{tc}} M_{n+m}, \tag{13}$$

or by disproportionation,[6,19]

$$M_n^{\bullet} + M_m^{\bullet} \xrightarrow{k_{td}} M_n + M_m. \tag{14}$$

On the basis of these observations, the rate of termination R_t can then be given by

$$R_t = k_t[M^{\bullet}]^2, \tag{15}$$

where $k_t = k_{\text{tc}} + k_{\text{td}}$ is the termination constant, and $[M^{\bullet}]$ is the total concentration of all chain radicals of size $M_1^{\bullet}$ and larger.[19] For low-monomer conversions we assume that the rate of radical formation equals the rate of radical disappearance (Bodenstein steady-state principal[19]); this is

also the case at low-monomer conversions, i.e., when only a little monomer is used up, $[I] \approx [I_{ic}]$, where $[I_{ic}]$ is the initial initiator concentration. Although we assume here that the rate at which the radicals are suppressed, k_ρ, is constant, the rate may differ during exposure. Reaching steady state in this process implies that the rate of initiation R_i and the rate of termination R_t are equal, yielding

$$fk_d[I] - R_\rho = k_t[M^\bullet]^2. \tag{16}$$

Solving for $[M^\bullet]$ we obtain

$$[M^\bullet]_{\text{stat}} = \left(\frac{fk_d[I] - R_\rho}{k_t} \right)^{1/2}, \tag{17}$$

where $[M^\bullet]_{\text{stat}}$ is the total concentration of all chain radicals of size $M_1^\bullet$ and larger at steady state. Assuming that much more monomer is consumed due to propagation polymerization than in the initiation reaction, the propagation rate R_{pg} [the rate of reaction of relation (4)] is approximately equal to the polymerization rate R_p; therefore

$$R_p \cong -\,\mathrm{d}[M]/\mathrm{d}t = k_p[M^\bullet][M]. \tag{18}$$

Substituting into Eq. (18) from Eq. (17) for $[M^\bullet]$ yields

$$R_p = k_\rho \left(\frac{fk_d[I] - R_\rho}{k_t} \right)^{1/2} [M]. \tag{19}$$

Examining the photochemical formation of free radicals, there are a number of initiation mechanisms,[20] many involving a photochemical electron transfer reaction. If we reexamine the way in which the monomer radicals are formed, we see that they are dependent on the quantity of free radicals formed per photon absorbed and the intensity of the light used for recording. As the inhibitor present indirectly consumes some of the absorbed photons, there is a reduction in the number of free radicals available for the initiation of monomer radicals and thus for the formation of polymer chains. The rate of initiation R_i can therefore be given by

$$R_i = f(\Phi' - R'_\rho)I_a = \Phi I_a - R_\rho, \tag{20}$$

where Φ' is the total number of radicals produced per photon absorbed and R'_ρ is the decrease due to the presence of oxygen. I_a is the intensity of light absorbed in moles of light quanta per liter per second and Φ is the total number of propagating chains that would be initiated per light photon absorbed if no inhibition took place.[6,17] As only a fraction f of the free radicals, which are produced, reacts with the monomer in the starting reaction, the cage effect has been included. R'_ρ indicates that the process of production of radicals, which cannot produce chains due to the cage effect, may still undergo inhibition.

Let us assume cosinusoidal spatially modulated illumination, i.e., $I(x) = I_0[1 + V\cos(Kx)]$ where V is the fringe visibility; $K = 2\pi/\Lambda$, the grating vector magnitude, and Λ is the grating period. The concentration of photosensitizers is related to the absorbed intensity by Beer's law:[19]

$$I_a(x,t) = I(x)\{1 - \exp[-\epsilon Z(t)d]\} = I(x)[1 - T(t)], \tag{21}$$

where ϵ is the molar absorptivity, $Z(t)$ is the time-dependent concentration of the photosensitizers (initiators), and d is the photopolymer layer thickness. Since the concentration of photosensitizers is a function of time, the transmittance of the layer $T(t)$ (Refs. 7 and 8) also depends on time and is discussed below. The concentration of free radicals given in Eq. (17) can now be written as

$$[M^\bullet] = \left\{ \frac{f(\Phi' - R'_\rho)I(x)[1 - T(t)]}{k_t} \right\}^{1/2}. \tag{22}$$

Therefore the polymerization rate from Eq. (19) is given by

$$R_p = k_p[M]\left\{ \frac{f(\Phi' - R'_\rho)I(x)[1 - T(t)]}{k_t} \right\}^{1/2} = \kappa(t)[M][I(x)]^{1/2}, \tag{23}$$

where $\kappa(t) = \kappa_0(t)A(t)^{1/2}$, $A(t) = 1 - T(t)$, $\kappa_0(t) = k_p[\Phi(t)/k_t]^{1/2}$, and $\Phi(t) = f(\Phi' - R'_\rho)$.

We can summarize the above as follows: $A(t)$ tells us the fraction of the incident light absorbed, Φ' tells us the fraction of this absorbed light that results in initiation, and finally $\Phi(t)$ tells us the fraction of photons that lead to polymerization.

The inclusion of the transmittance $T(t)$ allows a time-varying model for the polymerization rate R_p to be obtained. At the start of exposure the transmittance of the exposing light will be small due to the high absorbance of the photosensitive dye. This high absorption results in large values of $I_a(x,t)$ and of the polymerization rate factor $\kappa(t)$, and therefore a high rate of polymerization R_p. Similarly, as the transmittance of the layer increases during the exposure, both the light absorbed by the photopolymer material layer and the polymerization rate constant decrease, resulting in a lower rate of polymerization R_p.

To estimate $T(t)$, several transmittance curves were experimentally obtained for differing exposure intensities in our standard material layer.[1,7] There is an initial nonzero transmittance at the beginning of exposure as the material is never completely opaque. The transmittance function $T(t)$ was then determined based on fits to the experimental data. In Section 3 we introduce a loss fraction B to allow for nonabsorptive losses, i.e., Fresnel boundary reflections. $T(t)$ is estimated by fitting with the function

$$T(t) = E + G[1 - \exp(-a_0 t + a_1 t^2)], \tag{24}$$

where E, G, a_0, and a_1 are constant parameters related to the exposure intensity and the initial transmittance of the layer. Equation (24) is used in our numerical simulations, and some typical parameter results (and fitting errors) for different exposing intensities are given in Table 1.

In this section we have derived, for the first time to our knowledge, the rate equations governing the photochemical processes involved in grating formation that include a term to explicitly account for radical suppression due to the effect of inhibition, which we have assumed to be caused mainly by oxygen. Furthermore, following the work of Blaya *et al.*,[8] time dependence for the absorbance of the photosensitive dye and photoinitiators is included in our rate equations.

Table 1. Extracted Physical Parameters Obtained from Fits to the Data[a]

Parameter	Case 1	Case 2	Case 3
I_0 (mW/cm^2)	3.5	4.5	5.0
E (mW/cm^2)	0.857	1.124	1.636
G (mW/cm^2)	1.517	1.831	2.143
a_0 (s^{-1}) ($\times 10^{-2}$)	6.238	7.321	8.397
a_1 (s^{-2}) ($\times 10^{-4}$)	0.891	1.211	3.623
MSE[b] ($\times 10^{-3}$)	4.48	5.09	5.15
t_i (s)	0.41	0.21	0.13
κ ($cm^2\,mWs^{-1}$)	0.109	0.027	0.039
D (cm^2/s) ($\times 10^{-11}$)	3.0	2.5	3.5
C (cm^3/mol) ($\times 10^{-6}$)	3.1	5.5	6.1
MSE ($\times 10^{-10}$)	0.32	1.72	1.26

[a]See also Fig. 3.

[b]Mean square error.

3. POLYMERIZATION-DRIVEN DIFFUSION

In this section the basic theory behind grating growth will be presented. Following Galstyan *et al.*,[14] we incorporate the presence of inhibition and time-varying absorption effects in the material, as discussed in Section 2, into a local PDD model.[2]

A dry photopolymer layer typically consists of a monomer, binder, cross-linker, an electron donor, and a photoinitiator. As the material is exposed to the recording beams, the monomer is polymerized, and the amount of polymerized monomer increases with the exposure. In our material more monomer is polymerized in the bright fringes of the interference pattern than in the dark fringes. This results in a higher concentration of monomer in the dark regions than in the bright, and therefore a spatial monomer concentration gradient. The excess monomer will tend to diffuse into the bright regions.[2–6,19] The governing one-dimensional diffusion equation is

$$\frac{\partial u(x,t)}{\partial t} = \frac{\partial}{\partial x}\left[D(x,t)\frac{\partial u(x,t)}{\partial t} \right] - F(x,t)u(x,t), \qquad (25)$$

where $u(x,t)$ is the monomer concentration, $D(x,t)$ is the diffusion constant, and $F(x,t)$ is the polymerization rate. Equation (25) is Fick's law with the addition of a driving function representing the physical effects of the photopolymerization. The light intensity in the material is assumed periodic and is described by

$$I(x,t) = I_0[1 + V\cos(Kx)], \qquad (26)$$

with I_0 the average irradiance. In Section 2 we derived an equation governing the resulting polymerization rate. It is proportional to the exposure irradiance raised to $\gamma = 1/2$ (Ref. 21):

$$F(x,t) = F_0(t)[1 + V\cos(Kx)]^{\gamma} A^{\gamma}(t), \qquad (27)$$

where $A[t]$, the time-varying absorbance of the material,[8,9,22] has been included in the expression for the polymerization rate to account for the change in absorbed intensity during exposure. To account for the nonabsorptive losses present, a loss fraction B has been included by defining the polymerization rate parameter as $F_0(t) = \kappa_0(t) I_0^{\gamma}(1-B)$. The value of the loss fraction B is empirically obtained by repeated measurement of the losses in the layers and plates when all the monomer is polymerized and the dye is bleached, assuming that the nonabsorptive losses can be obtained. The expression for the polymerization rate parameter also includes the time-varying function $\kappa_0(t)$, which we introduce to model the inhibition period present at the start of exposure.[16–18,22,23]

For the $I(x,t)$ in Eq. (26), the monomer concentration can be written as a cosine series

$$u(x,t) = \sum_{i=0}^{\infty} u_i(t)\cos(iKx). \qquad (28)$$

This is substituted into Eq. (25) with the initial condition that $u(x,0) = U_0$, where U_0 is the initial uniform monomer concentration in the material. In our analysis we assume that harmonics of an order greater than 2, $i > 2$, can be neglected, i.e., their contributions are assumed negligible in comparison with that of the first three terms.[2] A set of first-order coupled differential equations, in terms of the monomer concentration harmonic amplitudes, is obtained.[2,14]

We now examine the $F_0(t)$ term appearing in Eq. (27) using the result from Section 2. From repeated observations of our experimental results, we know that grating growth is negligible for some period of time at the start of exposure. This appears to be primarily due to the action of inhibitors, such as oxygen,[14] which suppress the creation of free radicals. The process is as follows:

(i) the photosensitive dye is excited by the exposing photons;

(ii) the excited dye then reacts with the monomer generating free radicals;

(iii) this leads to the formation of polymer chains,[14] and then

(iv) the inhibitor acts to deactivate the dye from its excited state, stopping radical creation.

Although this process continually takes place during grating formation, it is most obvious (and most easily observed) at the beginning of exposure due to the high inhibitor concentration and the low concentration of excited dye.[23] As exposure proceeds, the suppression of radicals becomes less visible. We model this sharp temporal-state transition using a step function[14] $\Theta[x]$, where

$$x = U_0/i_d - \rho(t). \tag{29}$$

Here $\rho(t)$ is the concentration of oxygen present in the material, and i_d specifies by how much the monomer concentration must be greater than that of the oxygen for polymerization to occur. The fraction U_0/i_d acts to define a threshold (time after onset of exposure), at which polymerization begins to take place. The polymerization rate in Eq. (27) becomes

$$F(x,t) = \kappa I_0^{\gamma}(1-B)\Theta[U_0/i_d - \rho(t)][1 + V\cos(Kx)]^{\gamma}A^{\gamma}(t), \tag{30}$$

where $\kappa I_0^{\gamma}(1-B)\Theta[U_0/i_d-\rho(t)]=F_0(t)=\kappa_0(t)I_0^{\gamma}(1-B)$.

In describing the behavior of the dye, we make three assumptions about the kinetics:

(a) The diffusion rate of oxygen within the material and from the atmosphere into the layer is much higher than the rates of diffusion of all other materials present. Therefore the oxygen is able to instantaneously maintain a constant distribution.

(b) After the reaction with the dye it is assumed that the active inhibiting oxygen becomes an inert component, referred to in relation (7) as the photoreduction product Y, which has no further influence on the polymerization of the monomer.[14]

(c) The rate of change of the concentration of the active oxygen during exposure is assumed to be directly proportional to the total concentration of active oxygen.

From assumption (c), the differential equation governing the concentration of inhibiting oxygen can be written as

$$\frac{d\rho(t)}{dt} = -\beta'\rho(t), \tag{31}$$

where $\beta' = k' I_0(1-B)$ is a constant that is proportional to the average recording intensity, where k' is a material constant at a fixed temperature. The solution to Eq. (31) is

$$\rho(t) = \rho_0 \exp[-k' I_0(1-B)t], \tag{32}$$

where ρ_0 is the initial oxygen concentration. We substitute this into Eq. (30), which is in turn substituted into Eq. (25) along with Eq. (28) giving a set of first-order coupled equations.[2–6,14] Truncated equations, governing the monomer harmonic amplitudes, are obtained, i.e.,

$$\frac{du_0(\xi)}{d\xi} = -H(\xi)A(\xi)u_0(\xi) - \frac{1}{2}H(\xi)A(\xi)Vu_1(\xi), \tag{33}$$

$$\frac{du_1(\xi)}{d\xi} = -H(\xi)A(\xi)Vu_0(\xi) - \{H(\xi)A(\xi) + R \times \exp[-\alpha H(\xi)\xi]\cosh[\alpha H(\xi)V\xi]\}u_1(\xi), \tag{34}$$

where

$$\xi = \kappa I_0^{1/2} t, \quad R = \frac{DK^2}{f_0},$$

$$H(\xi) = \Theta\left[\frac{U_0}{i_d} - \rho_0 \exp\left(-\frac{k'(1-B)}{\kappa}\xi\right)\right],$$

$$A(\xi) = 1 - T(\xi).$$

We have assumed that D is the initial unchanged diffusion constant and $\alpha = 0$.[2–6]

The rate at which the concentration of polymer varies is proportional to the instantaneous rate of removal of monomer; thus $N(x,t)$, the polymerized monomer concentration at time t, is

$$N(x,t) = \int_{t_i}^{t} F(x,t')u(x,t')dt'. \tag{35}$$

We have observed that $N(x,t\leqslant t_i)=0$, due to inhibition, gives the lower limit on the integral t_i. While some photopolymerization may occur when $0<t\leqslant t_i$, it is assumed negligible; thus the step function provides a useful first-order description of the inhibition process. We substitute Eqs. (27) and (28) into Eq. (35) and write $N(x,t)$ as

$$N(x,t) = \sum_{i=0}^{2} N_i(t)\cos(iKx). \tag{36}$$

For volume (thick) holographic gratings replayed on Bragg,[24–26] it is the N_1 harmonic that diffracts the incident light. Therefore

$$N_1(\xi) = \int_0^{\xi} H(\xi')A(\xi')\left[Vu_0(\xi') + u_1(\xi') + \frac{1}{2}Vu_2(\xi')\right]d\xi. \tag{37}$$

Coupled-wave theory[27] predicts a relationship between the diffraction efficiency and the refractive index modulation of a sinusoidal thick transmission grating. Assuming that N_1 determines the amplitude of the grating refractive index modulation, $\Delta n = CN_1$ for some constant C.[3] The diffraction efficiency $\eta(\xi)$ of the grating is

$$\eta(\xi) = \sin^2\left[\frac{\pi d}{\lambda\cos\theta}CN_1(\xi)\right], \tag{38}$$

where d is the thickness of the material layer, λ is the wavelength of the probe–replay laser, and θ is the Bragg angle associated with that wavelength.[28]

We note that a much more complex relationship exists between the N_i and the Δn_i values,[29,30] and that while Eq. (38) holds for thick volume gratings, in general a rigorous electromagnetic model is needed to calculate the diffraction efficiency.[6]

4. POLYMERIZATION-DRIVEN DIFFUSION SIMULATIONS

We wish to apply our new model to characterize our material behavior by fitting experimental growth curves. Before carrying out this procedure we wish to examine the general behavior predicted by our model.

First we examine how the initial inhibition period is affected by changes in the oxygen concentration and the exposing intensity. Combining Eqs. (29) and (32) we obtain

$$t_i = \frac{1}{k' I_0 (1 - B)} \ln\left(\frac{i_d \rho_0}{U_0}\right). \quad (39)$$

We can find t_i using the experimentally reasonable parameter.[14] Examining Eq. (39) it is clear that t_i decreases as the concentration of oxygen present in the material decreases. By increasing the average exposure intensity I_0, the concentration of oxygen can be reduced at a quicker rate and this will result in a reduction of t_i. Equation (39) suggests that by using sufficiently strong exposure intensities, the presence of the initial dead band could be completely removed. Furthermore Eq. (39) can be used to determine the initial concentration of oxygen ρ_0, which is present in the material.

Second we examine the behavior of the harmonics of monomer concentration, and plots of the first three harmonics were generated. The results are plotted in Fig. 1 for an average exposure intensity of $I_0 = 3.5$ mW/cm^2. The following parameter values were used: $R = 1$, $V = 1$, $\alpha = 0$, $\kappa = 0.3$ cm^2 mWs^{-1}, and $k' = 0.1$ cm^2 mWs^{-1}. The initial monomer concentration was taken as $U_0 = 3.2$ g/l and $i_d = 100$. A value for the loss fraction was empirically found to be $B = 0.2 \pm 0.05$. The absorbance function $A(t)$ is defined using Eq. (24) and the transmittance parameter values used can be seen in case 1, Table 1. The initial oxygen concentration present in the layer was chosen to be $\rho_0 = 0.03$ g/l. This estimated value appears reasonable relative to the densities and volumes of the other materials present.[14] We note the presence of the initial dead band in Fig. 1 with $t_i \sim 1$ s.

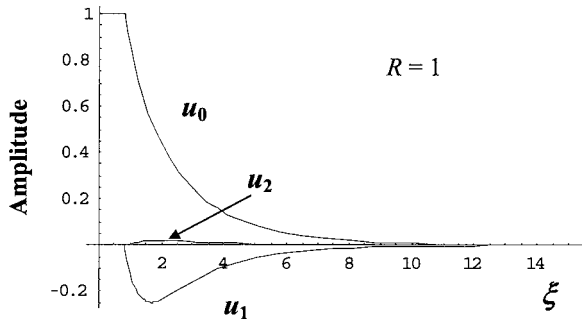

Fig. 1. First three Fourier harmonics of monomer concentration versus ξ, $R = 1$.

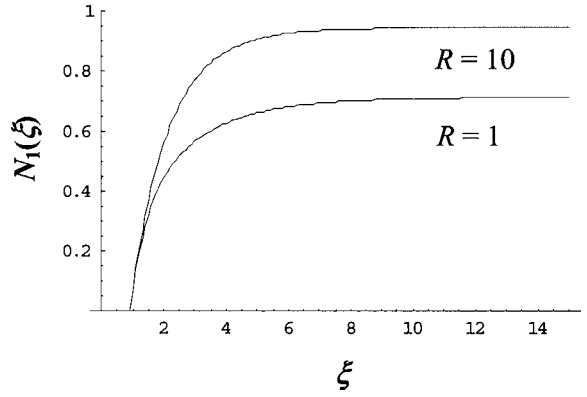

Fig. 2. N_1, first harmonic of polymer concentration versus ξ for $R = 1$ and $R = 10$. These values were chosen as being similar to the extracted experimental results.

Figure 2 shows the predictions for the first harmonic of the polymer concentration N_1 for the cases when $R = 1$ and 10. These values were chosen to illustrate the experimentally observed range of R values obtained. As can be seen, the larger the R value, the larger the N_1 saturation value. Once again we note the presence of the inhibition period at the start of exposure due to inhibition.

5. EXPERIMENTAL RESULTS, NUMERICAL FITTING, AND PARAMETER ESTIMATION

There are three parts to this section. First, in Subsection 5.A, we attempt to examine the effects of exposure intensity changes on the inhibition period to verify the predictions made using Eq. (39). Second, in Subsection 5.B, we discuss preexposure and note that a minimum dead-band duration is found to exist independent of the exposing intensity. Finally, in Subsection 5.C, we examine the effects of cover plating (sealing) on the inhibition effects. In all cases standard materials[1,7] and holographic exposing setups[28] were used. We added 16 cm^3 of Methylene Blue of concentration 1.25×10^{-3} M to the standard polyvinyl alcohol–acrylamide mix[1] to produce dry layers of thickness $d \sim 100 \pm 10$ μm.[7,28]

Fits to the experimental data presented in this section were performed using the model described in Section 3 applying the numerical fitting algorithm described in Refs. 1 and 6.

A. Intensity Effects

Figure 3 contains three growth curves for three different average exposure intensities $I_{01} = 3.5$ mW/cm^2, $I_{02} = 4.5$ mW/cm^2, and $I_{03} = 5$ mW/cm^2. The gratings were all recorded using a He–Ne laser with $\lambda = 633$ nm, $\Lambda = 1$ μm, and probing at $\lambda = 532$ nm (Refs. 1 and 7) with the same setup as that used in Refs. 7 and 28. As expected, the rate of polymerization increases with increasing exposure intensity. It is also noticeable that there is a decrease in the inhibition period.[15–18] The corresponding inhibition periods for the three intensities are $t_{i1} = 0.41$ s, $t_{i2} = 0.21$ s, and $t_{i3} = 0.13$ s, respectively. The results are in agreement with the predictions of Eq. (39). The dye molecules within the material are excited at a faster rate due to the increase in the intensity entering the material. This causes the oxygen present in the material to be removed at a quicker rate, as described by the rate equations in

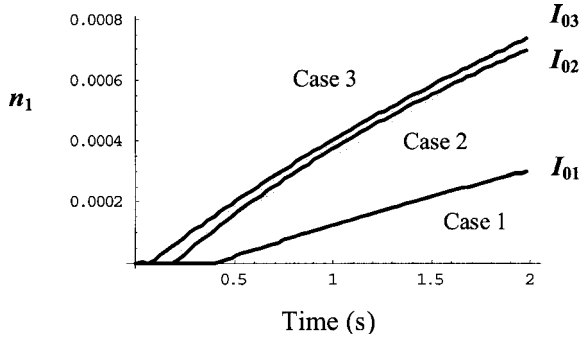

Fig. 3. Refractive index amplitude growth curves, showing the changes in the rate of polymerization for three different exposure intensities: theoretical fit (solid curves) and experimental data (dotted curves).

Section 2. This reduces the radical suppression, caused by the oxygen, and hence there is a decrease in the duration of the dead band caused by inhibition.

Since in Eq. (39) the $\beta' = k' I_0(1-B)$ term is a function of the average exposure intensity I_0, we can estimate values for i_d for different exposing intensities. From the experimental data presented in Fig. 3 we can extract values for the inhibition times; and by substituting reasonable values for U_0, k', ρ_0, I_0, and B, we can estimate i_d. These values can then be used during the data fitting procedure.

Applying a numerical least-squares algorithm we obtain best fits to the experimental data for the mean squared errors (MSEs) shown in the lower part of Table 1. We fit by first substituting known parameter values, i.e., $U_0 = 3.2$ g/l, $i_d = 85$, $\rho_0 = 0.03$ g/l, $k' = 0.1$ cm^2 mWs^{-1}, and $B = 0.2$, into our equations and then interactively testing the fit quality over reasonable ranges of the unknown parameters. In this way estimates for D (the diffusion coefficient), κ (the polymerization rate constant), and C are extracted. In Fig. 3 the solid curves are the theoretical fits to the data points. Typically the loss fraction is measured to have values in the range $B = 0.2 \pm 0.05$. We note that using values over this range does not appreciably vary the quality of the fits achieved (the calculated MSE values).

The resulting physical parameters are summarized in the lower part of Table 1. It can be seen that, as the exposure intensity is increased, the inhibition time decreases as expected. We note that the values for the diffusion constant D are comparable with previous results,[1,3–5,30] and the diffusion constant values of water and propanol reported recently.[31] The C values estimated are also comparable with previous results.[29] As can be seen in the lower part of Table 1, the resulting MSE values are small, which is also evident in the quality of the fits in Fig. 3. However, the estimated values for the polymerization rate constant κ vary significantly from case to case. This variation occurs due to the breakdown of the model. For example, all nonlocal material effects (temporal and spatial) have been neglected.[29] A step function has been used as a first-order approximation to model the threshold effect created by the inhibition process.[14] Furthermore the mechanism of chain termination is assumed to be bimolecular ($\beta = 1$).[5,8,29] Recently, we have indicated[5] that better fits can be achieved when a primary termination mechanism is used ($\beta = 2$).

B. Minimum Dead Band and Preexposure

We have observed experimentally that increasing the exposure intensity above some fixed value results in no further discernible reduction in the dead band. Where we increased the average holographic exposure intensity above 6 mW/cm^2 in our experiments, no further reduction of the initial inhibition period took place. We will discuss some possible explanations for the existence of this minimum dead band in Subsection 5.C. But first we note that it would seem reasonable to expect that by preexposing the material, dye molecules will become excited and reduce the concentration of active oxygen causing radical suppression. At this point, with all inhibition processes (i.e., active oxygen) eliminated, it should be possible for uninhibited holographic recording to take place.

In Fig. 4 the grating refractive index modulation, extracted from three different diffraction-efficiency grating-growth curves, are presented. In each case the polymer layer was preexposed, prior to holographic exposure, by a uniform plane wave with a preexposure intensity of $I_{PE} = 1.5$ mW/cm^2. The preexposed region on the plate was twice that of the area undergoing holographic grating exposure. This was done to ensure that there was no oxygen in the surrounding layer to diffuse into the area in which grating formation is taking place. The holographic exposure started almost immediately after the preexposure was complete, a typical delay of 0.5 s occurred, and in all cases a holographic exposure intensity of 3.5 mW/cm^2 was used. Curves 3, 2, and 1 are the growth curves of the gratings recorded with preexpose durations of 3, 2, and 1 s, respectively.

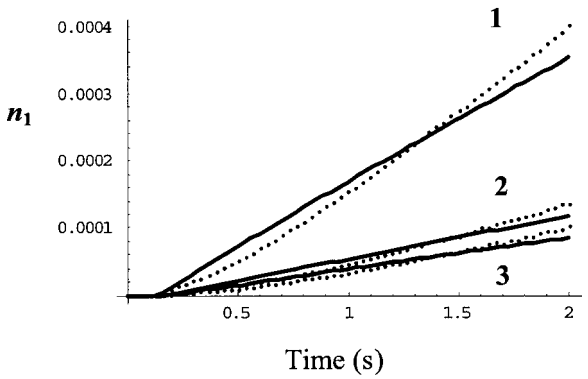

Fig. 4. Growth curves with varying preexposure times of 3, 2, and 1 s: theoretical fit (solid curves) and experimental data (dotted curves). There are changes in the inhibition periods and the rates of polymerization.

It can be seen in Fig. 4 that preexposure reduces the rate of polymerization. This may arise because preexposure bleaching means that less dye is available at the start of the holographic exposure. Importantly we note from Fig. 4 that the inhibition period does not seem to change significantly with the preexposure. This would appear to suggest that the active oxygen, which is removed before the start of the holographic exposure by the preexposure, is being rapidly replaced from the air above the plate. If oxygen is constantly and rapidly diffusing into the layer, then the suppression of radicals is continuously taking place and reducing the rate of photopolymerization at all times during the exposure.

Fits to the experimental data presented in Fig. 4 were obtained (solid curves). The values for the transmittance and material parameters used are those given in Subsection 5.A and Table 1 for the holographic exposure intensity, $I_0 = 3.5$ mW/cm^2. This intensity was chosen to allow the inhibition period to be easily observed. The resulting extracted physical parameters obtained for the data in Fig. 4 are summarized in Table 2. Once again disagreements between the experimental and theoretical results can be explained in terms of the deficiencies of our models.

C. Cover Plating

From the experiments described above we have identified the effects on the inhibition period and on the rate of polymerization of the average holographic exposure inten-

Table 2. Physical Parameter Values Obtained from Fits to the Data in Fig. 4

Time (s)	ρ_0 (g/l)	i_d	t_i (s)	κ (cm^2 mWs^{-1})	D (cm^2/s) ($\times 10^{-11}$)	C (cm^3/mol) ($\times 10^{-6}$)	MSE ($\times 10^{-8}$)
1	0.0400	87.0	0.30	0.0100	4.54	2.6	25
2	0.0376	92.0	0.22	0.0070	4.52	0.94	3.8
3	0.0355	95.2	0.15	0.0067	4.52	0.69	2.2

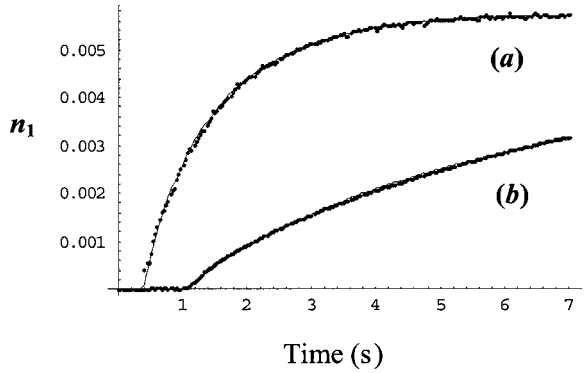

Fig. 5. Fit to the experimentally obtained growth curve of refractive index amplitude versus exposure time for (a) cover-plated material layer preexposed for 1 s and (b) uncover-plated material layer without preexposure: theoretical fit (solid curves) and experimental data (dotted curves).

sity and of preexposure. However, to explain the continuing existence of a minimum dead band, which is observed in Fig. 4, we have proposed that a significant amount of oxygen is diffusing into the material from the air. In an effort to eliminate the effects of such diffusion, we cover plated the material using an index-matched fluid, silicon oil, and a glass plate. Figure 5 contains two growth curves. Curve (a) is for a sealed plate that has been preexposed for 1 s with a preexposure intensity of $I_{PE}=1.5$ mW/cm^2 and then, within 0.5 s, holographically exposed with an average exposure energy of $I_0=3$ mW/cm^2. Curve (b) is for an unsealed plate that was not preexposed. In both cases identical holographic exposure is taking place. While a significant reduction in the inhibition dead band can be seen to have taken place in curve (a), it has not, however, been completely eliminated.

At the start of Subsection 5.B we indicated the existence of a minimum inhibition dead-band duration. Let us assume that the excitation of the dye by light is instantaneous. It would seem possible that the remaining dead band is due to an induction period[19] associated with the initial stages of free radical polymerization. If polymer chain growth does not occur instantaneously, this will lead to a corresponding delay in grating formation, which accounts for the remaining dead band. This effect will continue to occur even after the effects of the inhibitor are removed. Although increasing the intensity used to record a grating can reduce the induction period, it cannot be completely eliminated in this way.[19]

Examining Fig. 5, the initial rate of polymerization in curve (a) is larger than that in curve (b). We have experimentally observed that the relaxation of the bleached dye requires times significantly longer than the 0.5 s delay employed by us between preexposure and holographic exposure. Therefore the reduction in the rate of photopolymerization, which arises due to the reduced concentration of unbleached dye, appears to be significantly less than the rate reduction arising due to the presence of oxygen.

For both sets of data, fitting is performed using the same material parameter values used in Fig. 3. However since $I_0=3$ mW/cm^2, the transmittance parameters used are different: $E=0.7656$ mW/cm^2, $G=1.45$ mW/cm^2, $a_0=4.45\times10^{-2}$ s^{-1}, and $a_1=0.361\times10^{-4}$ s^{-2} extracted from a fit with an MSE$=4.01\times10^{-3}$. The loss fraction value used to produce the fits shown in Fig. 5 are (a) $B=0.3$ and (b) $B=0.2$. The reason for the difference in the loss fraction for the two cases is the change in the amount of light lost due to the extra reflective surfaces in the cover plate. Once again errors in the B values (±0.05) do not effect the quality of the resulting growth curve fits.

The resulting extracted physical parameters are summarized in Table 3. Clear differences between the numerical estimates of the various polymerization rates and inhibition periods are found. The good agreement between the experimental data and theoretical fits can be seen in Fig. 5 and are quantitatively supported by the low MSE values presented in Table 3.

We believe that Fig. 5 illustrates most clearly the significance of effects studied in this paper. Comparing the two growth curves, it can be seen that for particular holographic exposure intensities, the inhibition period can be reduced to a minimum induction period value by a combination of preexposure and cover plating. This reduction is accompanied by an increase in the rate of polymerization.

While the values obtained for the diffusion rate D and the constant C are consistent with values presented in the literature,[3–5,29] once again it can be seen that the polymerization rate constant values vary significantly. Once again we attribute this to the assumptions made in deriving our model and we are currently working to generalize our model.

6. CONCLUSIONS

Starting with a detailed description of the photochemical processes taking place in acrylamide-based photopolymer materials, we have developed a polymerization-driven diffusion model (PDD), which includes the effects of oxygen-based inhibition and dye absorption during grating formation. Including these effects has increased our ability to predict the time evolution of grating formation during exposure. The resulting understanding has allowed us to improve material performance appreciably via a combination of preexposure and cover plating.

Table 3. Values Obtained from Fits to the Data Sets in Fig. 5

	t_i (s)	κ (cm^2 mWs^{-1})	i_d	ρ_0 (g/l)	D (cm^2/s) ($\times 10^{-11}$)	C (cm^3/mol) ($\times 10^{-5}$)	MSE ($\times 10^{-10}$)
Cover plated and preexposed (1 s)	0.25	0.200	92	0.0355	2.0	6.06	0.95
Not cover plated, no preexposure	1.10	0.055	120	0.0400	2.5	2.04	1.50

Experimentally we have explored the behavior of the inhibition period. We have shown that this initial dead-band period can be reduced, although not eliminated, using strong holographic exposing intensities. We have experimentally observed both a decrease in the inhibition period and an increase in the rate of polymerization using a combination of preexposures and cover plating to seal the dry layer. We have explained the minimum dead band as a photopolymerization induction period.

The model presented here has many limitations and these have been discussed. However, despite these drawbacks, we have succeeded in applying the model to provide plausible explanations for the observed results and to numerically extract reasonable estimates for several material parameters.

Much work remains to be done. One fundamental assumption made in this paper is that it is the reaction of oxygen with the excited dye molecules that leads to inhibition. It is also possible that inhibition may occur primarily at the radicalized monomer stage. While much work is still clearly needed in either of these cases, our simplified mathematical model, which stresses the suppression of chain initiation, will be of value.

The model for the time-varying absorption of the material also needs to be improved to include variations with depth.[9] The theoretical models for inhibition and absorption must be integrated into the nonlocal polymerization-driven diffusion model for both nonlocal time and spatial responses. A more exact expression for the refractive index modulation such as the Lorentz–Lorenz equation should be included.[29] Other effects such as the chain termination mechanisms and material shrinkage[8,29,32,33] must be included to enable a more accurate physical picture to emerge. In particular we note that our use of a step function to model the inhibition period must be reexamined. However, given the variety of material in which inhibition effects[23,34] and threshold effects[35] have been observed, even the incomplete results presented here are significant for a wide range of applications, including holographic data storage,[36–38] diffractive optical element fabrication,[39–41] and photoembossing.[32]

ACKNOWLEDGMENTS

We acknowledge the support of Enterprise Ireland and Science Foundation Ireland through the Research Innovation and Proof of Concept Funds, and the Basic Research and Research Frontiers Programs and the Irish Research Council for Science, Engineering and Technology.

The corresponding author is J. T. Sheridan: e-mail, john.sheridan@ucd.ie; phone, 353-1-716-1927; fax, 353-1 +283-0921.

REFERENCES

1. J. R. Lawrence, F. T. O'Neill, and J. T. Sheridan, "Photopolymer holographic recording material," Optik (Stuttgart) **112**, 449–463 (2001).
2. G. Zhao and P. Mouroulis, "Diffusion model of hologram formation in dry photopolymer materials," J. Mod. Opt. **41**, 1929–1939 (1994).
3. J. T. Sheridan and J. R. Lawrence, "Nonlocal-response diffusion model of holographic recording in photopolymer," J. Opt. Soc. Am. A **17**, 1108–1114 (2000).
4. J. R. Lawrence, F. T. O'Neill, and J. T. Sheridan, "Adjusted intensity nonlocal diffusion model of photopolymer grating formation," J. Opt. Soc. Am. A **19**, 621–624 (2002).
5. J. V. Kelly, F. T. O'Neill, and J. T. Sheridan, "Holographic photopolymer materials: nonlocal polymerization-driven diffusion under nonideal kinetic conditions," J. Opt. Soc. Am. B **22**, 407–416 (2005).
6. S. Wu and E. N. Glytsis, "Holographic grating formation in photopolymers: analysis and experimental results based on a nonlocal diffusion model and rigorous coupled-wave analysis," J. Opt. Soc. Am. B **20**, 1177–1188 (2003).
7. M. R. Gleeson, J. V. Kelly, F. T. O'Neill, and J. T. Sheridan, "Recording beam modulation during grating formation," Appl. Opt. **44**, 1–8 (2005).
8. S. Blaya, L. Carretero, R. F. Madrigal, M. Ulibarrena, P. Acebal, and A. Fimia, "Photopolymerization model for holographic gratings formation in photopolymers," Appl. Phys. B **77**, 639–662 (2003).
9. S. Gallego, M. Ortuno, C. Neipp, and J. T. Sheridan, "3-dimensional analysis of holographic photopolymers based memories," Opt. Express **13**, 3543–3557 (2005).
10. International Union of Pure and Applied Chemistry, *Compendium of Chemical Terminology*, 2nd ed. (Blackwell Scientific, 1997).
11. J. B. Birk, *Organic Molecular Photophysics* (Wiley, 1975), Vol. 2.
12. R. L. Sutherland, V. P. Tondiglia, L. V. Natarajan, and T. J. Bunning, "Phenomenological model of anisotropic volume hologram formation in liquid-crystal-photopolymer mixtures," J. Opt. A **96**, 951–965 (2004).
13. A. Gilbert and J. Baggott, *Essentials of Molecular Photochemistry* (Blackwell Scientific, 1991).
14. A. V. Galstyan, R. S. Hakobyan, S. Harbour, and T. Galstian, "Study of the inhibition period prior to the holographic grating formation in liquid crystal photopolymerizable materials," http://e-lc.org/Documents/Tigran_V_Galstian_2004_05_05_11_13_17.pdf.
15. S. Piazzolla and B. Jenkins, "Dynamics during holographic exposure in photopolymers for single and multiplexed gratings," J. Mod. Opt. **46**, 2079–2110 (1999).
16. D. J. Lougnot and C. Turck, "Photopolymers for holographic recording: II. Self-developing materials for real-time interferometry," Pure Appl. Opt. **1**, 251–268 (1992).
17. D. J. Lougnot and C. Turck, "Photopolymers for holographic recording: III. Time modulated illumination and thermal post-effect," Pure Appl. Opt. **1**, 269–279 (1992).

18. N. Noiret, C. Meyer, and D. J. Lougnot, "Photopolymers for holographic recording: V. Self-processing systems with near infrared sensitivity," Pure Appl. Opt. **3**, 55–71 (1994).
19. G. Odian, *Principles of Polymerization* (Wiley, 1991).
20. W. J. Tomlinson, "Organic photochemical refractive-index systems," in *Advances in Photochemistry* (Wiley, 1980).
21. J. H. Kwon, H. C. Chang, and K. C. Woo, "Analysis of temporal behavior of beams diffracted by volume gratings formed in photopolymers," J. Opt. Soc. Am. B **16**, 1651–1657 (1999).
22. C. Carre, D. J. Lougnot, and J. P. Fouassier, "Holography as a tool for mechanistic and kinetic studies of photopolymerisation reactions: a theoretical and experimental approach," Macromolecules **22**, 791–799 (1989).
23. R. K. Kostuk, "Dynamic hologram recording characteristics in DuPont photopolymers," Appl. Opt. **38**, 1357–1363 (1999).
24. R. R. A. Syms, *Practical Volume Holography* (Clarendon, 1990).
25. M. Born and E. Wolf, *Principles of Optics: Electromagnetic Theory of Propagation, Interference and Diffraction of Light*, 6th ed. (Pergamon, 1980).
26. E. Hecht, *Optics*, 2nd ed. (Addison-Wesley, 1987).
27. H. Kogelnik, "Coupled wave theory for thick holographic gratings," Bell Syst. Tech. J. **48**, 2909–2947 (1969).
28. F. T. O'Neill, J. R. Lawrence, and J. T. Sheridan, "Automated recording and testing of holographic optical element arrays," Optik (Stuttgart) **111**, 459–467 (2000).
29. J. V. Kelly, M. R. Gleeson, C. E. Close, F. T. O'Neill, J. T. Sheridan, S. Gallego, and C. Neipp, "Temporal analysis of grating formation in photopolymer using the nonlocal polymer driven diffusion model," Opt. Express **13**, 6990–7004 (2005).
30. I. Aubrecht, M. Miller, and I. Koudela, "Recording of holographic gratings in photopolymers: theoretical modelling and real-time monitoring of grating growth," J. Mod. Opt. **45**, 1465–1477 (1998).
31. C. E. Close, M. R. Gleeson, F. T. O'Neill, J. V. Kelly, and J. T. Sheridan, "Control and measurement of the physical properties in acrylamide based photopolymer materials," Proc. SPIE **5827**, 346–357 (2005).
32. F. T. O'Neill, A. J. Carr, S. M. Daniels, M. R. Gleeson, J. V. Kelly, J. R. Lawrence, and J. T. Sheridan, "Refractive elements produced in photopolymer layers," J. Mater. Sci. **40**, 4129–4132 (2005).
33. F. T. O'Neill, J. R. Lawrence, and J. T. Sheridan, "Thickness variation of self-processing acrylamide based photopolymer and reflection holography," Opt. Eng. **40**, 533–539 (2001).
34. K. Sukegawa, S. Sugawara, and K. Murase, "Holographic recording by Fe^{3+}-sensitized photopolymerization," Electron. Commun. Jpn. **58C**, 132–138 (1975).
35. S. Gallego, M. Ortuno, C. Neipp, A. Marquez, A. Belendez, E. Fernandez, and I. Pascual, "3-dimensional characterization of thick grating formation in PVA/AA based photopolymer," Opt. Express **14**, 5121–5128 (2006).
36. H. J. Coufal, D. Psaltis, and G. T. Sincerbox, eds., *Holographic Data Storage*, Springer Series in Optical Sciences Series (Springer, 2000).
37. J. T. Sheridan, M. R. Gleeson, J. V. Kelly, and F. T. O'Neill, "Nonlocal polymerization-driven diffusion-model-based examination of the scaling law for holographic data storage," Opt. Lett. **30**, 239–241 (2005).
38. S. Orlic, E. Dietz, S. Frohmann, Ch. Müller, and H. J. Eichler, "High density multilayer recording of microgratings for optical data storage," Proc. SPIE **5521**, 149–160 (2004).
39. H. Kobolla, J. T. Sheridan, E. Gluch, J. Schmidt, R. Völkel, J. Schwider, and N. Streibl, "Holographic 2-D mixed polarisation deflection elements," J. Mod. Opt. **40**, 613–624 (1993).
40. H. Kobolla, J. Schmidt, J. T. Sheridan, N. Streibl, and R. Völkel, "Holographic optical beamsplitters in dichromated gelatin," J. Mod. Opt. **39**, 881–887 (1992).
41. J. Schmidt, R. Völkel, W. Stork, J. T. Sheridan, J. Schwider, N. Streibl, and F. Durst, "Diffractive beam splitter for laser Doppler velocimetry," Opt. Lett. **17**, 1240–1242 (1992).